### **NANOMATERIALS**

# Direct synthesis and chemical vapor deposition of 2D carbide and nitride MXenes

Di Wang<sup>1</sup>, Chenkun Zhou<sup>1</sup>, Alexander S. Filatov<sup>1</sup>, Wooje Cho<sup>1</sup>, Francisco Lagunas<sup>2</sup>, Mingzhan Wang<sup>3</sup>, Suriyanarayanan Vaikuntanathan<sup>1</sup>, Chong Liu<sup>3</sup>, Robert F. Klie<sup>2</sup>, Dmitri V. Talapin<sup>1,3,4</sup>\*

Two-dimensional transition-metal carbides and nitrides (MXenes) are a large family of materials actively studied for various applications, especially in the field of energy storage. MXenes are commonly synthesized by etching the layered ternary compounds, called MAX phases. We demonstrate a direct synthetic route for scalable and atom-economic synthesis of MXenes, including compounds that have not been synthesized from MAX phases, by the reactions of metals and metal halides with graphite, methane, or nitrogen. The direct synthesis enables chemical vapor deposition growth of MXene carpets and complex spherulite-like morphologies that form through buckling and release of MXene carpet to expose fresh surface for further reaction. The directly synthesized MXenes showed excellent energy storage capacity for lithium-ion intercalation.

Xenes, where M stands for early transition metal (such as Ti, V, Nb, or Mo) and X is C or N, are a large family of two-dimensional (2D) transition-metal carbides and nitrides. Since the discovery of  $Ti_3C_2T_x$  (T = O, OH, and F) in 2011 (1), MXenes have been commonly synthesized from crystalline MAX phases (where A is typically Al, Si, or Ga) through selective etching of A atoms with hydrofluoric acid (HF)-containing solutions (1-3) or Lewis acidic molten salts (4, 5), followed by the delamination of the MXene sheets (6). Interest in MXenes continues to grow because of their potential applications in energy storage (7, 8), electromagnetic interference (EMI) shielding (9, 10), transparent conductive layers (11), superconductivity (5), and catalysis (12). Moreover, the aforementioned T components in MXenes can be replaced with covalently bonded surface groups, including organic molecules, either during etching of the MAX phases (4, 13), or through postsynthetic modifications of surface groups (5). As such, opportunities are available to combine the benefits of 2D MXenes, such as a low diffusion barrier for cation intercalation (14), excellent electrical and thermal conductivity (3), and nearly endless tailorability of molecular surface groups.

Preparations of MXenes through hightemperature synthesis and chemical etching of MAX (15) or non-MAX (16, 17) phases require high energy consumption, show poor atom economy, and use large amounts of hazardous HF or Lewis acidic molten salts. The development of direct synthetic methods would facilitate practical applications of the rapidly

<sup>1</sup>Department of Chemistry and James Franck Institute, University of Chicago, Chicago, IL 60637, USA. <sup>2</sup>Department of Physics, University of Illinois Chicago, Chicago, IL 60607, USA. <sup>3</sup>Pritzker School of Molecular Engineering, University of Chicago, Chicago, IL 60637, USA. <sup>4</sup>Center for Nanoscale Materials, Argonne National Laboratory, Argonne, IL 60439, USA. \*Corresponding author. Email: dvtalapin@uchicago.edu developing family of functional MXenes. An ideal approach would involve a reaction of inexpensive precursors into MXenes bypassing intermediate MAX phases. In 2019, Druffel  $et\ al.$  reported the synthesis of  $Y_2CF_2$  with a MXenelike structure from the solid-state reaction between  $YF_3$ , Y metal, and graphite (18), based on the previously reported synthesis of Sc, Y, and Zr metal carbide halides by  $Hwu\ et\ al.$  in 1986 (19).

Among about 100 known MXene structures, Ti MXenes show some of the best combinations of physical and chemical properties (20) relevant to a variety of applications (21). We show that Ti<sub>2</sub>CCl<sub>2</sub> and Ti<sub>2</sub>NCl<sub>2</sub> MXenes can be directly synthesized from Ti metal, titanium chlorides (TiCl3 or TiCl4), and various carbon or nitrogen sources, including graphite, CH4, or N<sub>2</sub>. The directly synthesized MXenes (denoted as DS-MXenes) can be delaminated, and their surface groups can be replaced with other molecules through nucleophilic substitution or completely removed by means of reductive elimination (5). Besides convenience and scalability, the direct synthesis routes offer synthetic modalities not compatible with traditional MAX etching methods. For example, we demonstrated chemical vapor deposition (CVD) synthesis of extended carpets of  $\rm Ti_2CCl_2, Ti_2NCl_2, Zr_2CCl_2,$  and  $\rm Zr_2CBr_2$  MXene sheets oriented perpendicular to the substrate. Such orientations make MXene surfaces easily accessible for ion intercalation (7, 22) and chemical or electrochemical transformations (23, 24) by exposing edge sites with high catalytic activity (25, 26).

# Direct synthesis of Ti<sub>2</sub>CCl<sub>2</sub> MXene

The synthesis of DS- $Ti_2CCl_2$  was accomplished through the high-temperature reaction between Ti, graphite, and  $TiCl_4$  (Fig. 1A). Titanium and graphite were ground into a fine powder in a 3:1.8 molar ratio and combined with 1.1 molar

equivalent TiCl<sub>4</sub>. The mixture was sealed quartz ampoule and heated to 950°C in 20 and the temperature was maintained a

and the temperature was maintained until the reaction was finished; typically, 2 hours is sufficient for maximum yield of MXene. The reaction could be performed on a multigram scale (fig. S1) and should be easily amenable to further scaling.

Powder x-ray diffraction (XRD) and structural analysis by means of Rietveld refinement of the as-synthesized reaction products (Fig. 1B) revealed the presence of a Ti<sub>2</sub>CCl<sub>2</sub> MXene phase with the lattice parameters a =3.2284(2) Å and c = 8.6969(1) Å (numbers in parentheses are standard uncertainties), which are near the values reported for Ti<sub>2</sub>CCl<sub>2</sub> MXene synthesized by etching of Ti<sub>2</sub>AlC MAX phase with Lewis acidic molten salt (referred to as MS-MXenes) (5). Cubic  $TiC_x$  (x = 0.5 to 1) was often present as a by-product but could be efficiently removed through its precipitation from nonaqueous dispersions of the raw product prepared, for example, by means of ultrasonic dispersion in propylene carbonate (PC) or delamination of DS-Ti<sub>2</sub>CCl<sub>2</sub> with n-butyllithium (n-BuLi) (Fig. 1C).

The formation of Ti<sub>2</sub>CCl<sub>2</sub> MXene was observed initially at ~850°C, and the yield of MXene was maximal at 950°C (fig. S2A). TiC<sub>x</sub> became the dominant reaction product at temperatures >1000°C. At 950°C, the formation of Ti<sub>2</sub>CCl<sub>2</sub> phase was observed after 2 hours, and the ratio between Ti<sub>2</sub>CCl<sub>2</sub> and TiC<sub>x</sub> in products did not change substantially after increasing reaction time from 2 hours to 10 days at this temperature (fig. S2B). This finding naturally raises a question whether MXene was the kinetic or thermodynamic product of the reaction. We noticed that MXene phase did not form when we attempted to react  $TiC_x$  with Ti and  $TiCl_3$  or  $TiCl_4$  (fig. S2C). However, prolonged heating of purified MS-Ti<sub>2</sub>CCl<sub>2</sub> at 950°C resulted in a partial conversion into  $\mathrm{TiC}_x$  (fig. S3). We concluded from these observations that Ti<sub>2</sub>CCl<sub>2</sub> was a kinetically favored phase forming in competition with  $TiC_x$ .

The XRD patterns of DS-Ti<sub>2</sub>CCl<sub>2</sub> synthesized from TiCl<sub>3</sub> or TiCl<sub>4</sub> were similar (fig. S4B), as were scanning electron microscopy (SEM) images of the products' morphology, represented by large MXene stacks (Fig. 1D and figs. S5 and S6). A high-resolution high-angle annular dark field (HAADF) scanning transmission electron microscopy (STEM) image of DS-Ti<sub>2</sub>CCl<sub>2</sub> oriented along the  $[2\overline{1}\overline{1}0]$  zone axis and its corresponding electron energy loss spectroscopy (EELS) elemental maps are shown in Fig. 1, F and G, respectively. The center-to-center distance between MXene sheets calculated from the HAADF image is  $0.87 \pm 0.06$  nm (fig. S7), which is in agreement with the value of 0.87  $\pm$ 0.02 nm measured with XRD on multiple samples. DS-Ti<sub>2</sub>CCl<sub>2</sub> MXene sheets contained Ti and

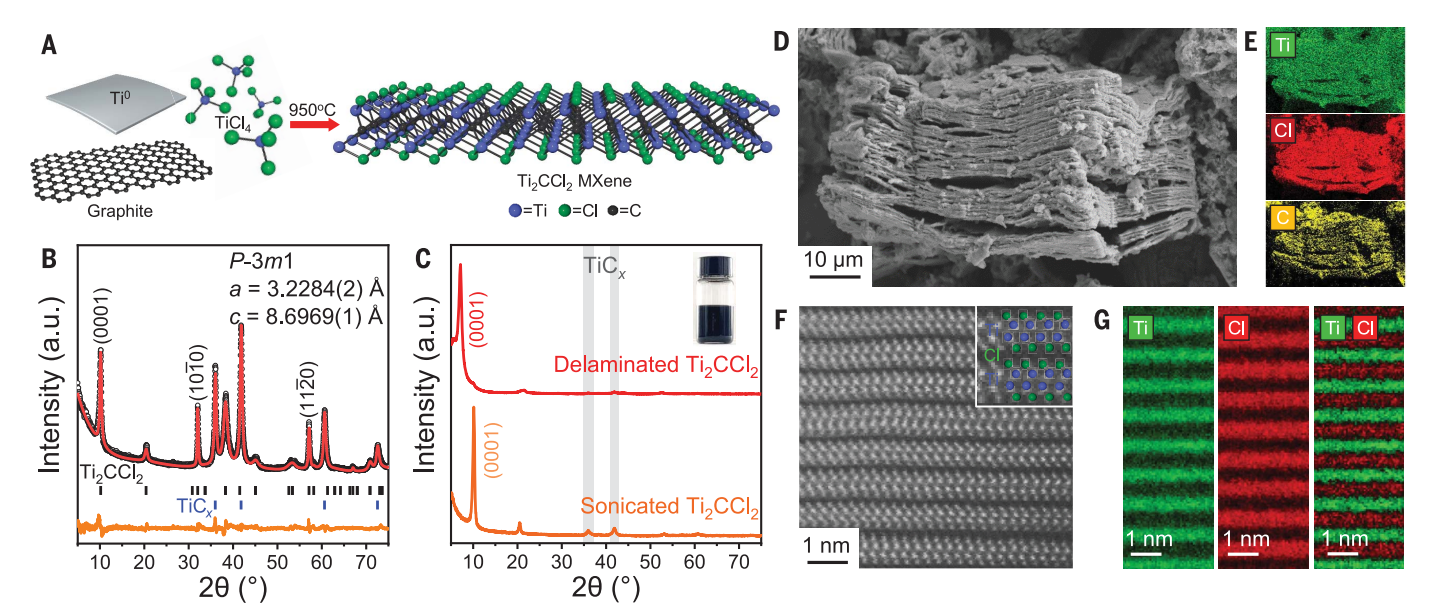


**Fig. 1.** Direct synthesis and characterization of DS-Ti<sub>2</sub>CCl<sub>2</sub> MXene. (A) Schematic diagram of the synthesis. (B) XRD pattern and Rietveld refinement of DS-Ti<sub>2</sub>CCl<sub>2</sub> prepared by reacting Ti, graphite, and TiCl<sub>4</sub> at 950°C. (C) XRD patterns of dispersible delaminated and sonicated DS-Ti<sub>2</sub>CCl<sub>2</sub>

MXenes. (Inset) Colloidal solution of the delaminated DS-Ti<sub>2</sub>CCl<sub>2</sub>. (**D**) SEM image and (**E**) EDX elemental mapping of a DS-Ti<sub>2</sub>CCl<sub>2</sub> stack. (**F**) High-resolution HAADF image and (**G**) EELS atomic column mapping representing the layered structure of DS-Ti<sub>2</sub>CCl<sub>2</sub>.

Cl with an atomic ratio of 49.9:50.1 (fig. S8), which is near the ideal 1:1 stoichiometry. This ratio suggested that the full coverage of MXene surfaces with Cl was achieved. In comparison, the MXenes synthesized by using the traditional MAX-exfoliation route are often deficient in surface coverage, with a typical stoichiometry of Ti<sub>2</sub>CCl<sub>1.5-1.7</sub> (5). The formation of Cl-terminated titanium carbide sheets was further confirmed by characteristic binding energies (fig. S9) in the x-ray photoelectron spectroscopy (XPS) (27). All these features, together with the assessment of crystal quality from linewidths in Raman spectra (fig. S10), confirmed the high degree of structural perfection of our DS-Ti<sub>2</sub>CCl<sub>2</sub> product.

As-synthesized DS-Ti<sub>2</sub>CCl<sub>2</sub> MXene stacks could be delaminated and solution-processed as individual 2D monolayers (Fig. 1C and fig. S11). For delamination, multilayer MXene was first intercalated with Li<sup>+</sup> by treatment with 2.5 M n-BuLi hexane solution (fig. S12A) (5, 28) then shaken with polar solvents such as Nmethylformamide (NMF) or 2,6-difluoropyridine (DFP) to form a suspension of delaminated 2D sheets (fig. S13). Insoluble by-products were selectively precipitated by a mild centrifugation at 240 g for 15 min (fig. S12B). In delaminated DS-Ti<sub>2</sub>CCl<sub>2</sub>, the (0001) diffraction peak shifted to a lower 2θ angle of 7.02°, corresponding to the enlarged d-spacing of 12.54 Å, from the original 8.70 Å. A similar d-spacing expansion was found in delaminated  $Ti_3C_2Cl_2$  MXenes (from 11.08 to 14.96 Å) (5). Delamination of DS-Ti<sub>2</sub>CCl<sub>2</sub> MXenes can be performed on a multigram scale, producing ~25 g·liter $^{-1}$  colloidal dispersions that can be stable for months under  $N_2$  atmosphere (fig. S14).

# CVD of MXenes

CVD is a versatile technique for synthesizing films, heterostructures, and complete devices by reacting gaseous precursors on a substrate. Although transition-metal carbides and nitrides such as  $\mathrm{Mo_2C}$ ,  $\mathrm{Mo_2N}$ , and  $\mathrm{TiC}_x$  can be grown with CVD (29–31), such a synthetic option has not been previously available for MXenes. We introduce the direct synthesis of MXenes through CVD and show a route to new morphologies of MXenes with more easily accessible surfaces and exposed catalytically active edges.

We grew MXenes by CVD at 950°C on a Ti surface with a CH4 and TiCl4 gas mixture diluted in Ar (Fig. 2A). After the exposure for 15 min, the as-synthesized product (denoted as CVD-Ti<sub>2</sub>CCl<sub>2</sub>) was characterized by means of XRD (Fig. 2B). According to the Rietveld refinement, the lattice parameters a = 3.2225(2) Åand c = 8.7658(8) Å matched well with the reported values for Ti<sub>2</sub>CCl<sub>2</sub> MXene (5). Raman spectra (Fig. 2C) also confirmed the purity of Ti<sub>2</sub>CCl<sub>2</sub> MXene. High-resolution STEM-EELS (fig. S15) and EDX analysis (fig. S16) confirmed the crystallinity and stoichiometry of CVD-Ti<sub>2</sub>CCl<sub>2</sub>. The center-to-center interlayer distance of  $0.88 \pm 0.05$  nm calculated from STEM images (fig. S17) was typical for Ti<sub>2</sub>CCl<sub>2</sub> MXenes. SEM images showed a substrate fully covered with a wrinkled layer of Ti<sub>2</sub>CCl<sub>2</sub> (Fig. 2D). Such a carpet of Ti<sub>2</sub>CCl<sub>2</sub> MXene sheets grown perpendicular to the substrate would be difficult for traditionally synthesized MXenes to achieve. This morphology, previously observed for other CVD-grown 2D materials such as  $MoS_2$  (32), appeared particularly promising for efficient ion intercalation, such as in supercapacitors (7, 22).

We used direct CVD synthesis to produce MXenes that have not been previously prepared by the etching of MAX phases. For example, Zr<sub>2</sub>CCl<sub>2</sub> and Zr<sub>2</sub>CBr<sub>2</sub> MXenes were synthesized by exposing a Zr foil to CH4 and ZrCl4 or ZrBr<sub>4</sub> vapor at 975°C. These two zirconium MXenes appeared in the same general morphology as that of the titanium MXenes, adopting vertically aligned carpet-like structure on the surface of the Zr foil (fig. S18). Arguably the most intriguing product of the direct synthesis was phase-pure nitride Ti<sub>2</sub>NCl<sub>2</sub> MXene formed through the reaction of Ti foil with TiCl4 and N<sub>2</sub> above 640°C (Fig. 2, A to C and E, and figs. S19 and S20). Nitride MXenes have been predicted to have a variety of attractive properties, including ferromagnetism and higher conductivity as compared with that of carbide MXenes (33). However, the challenge of making nitride MXenes by traditional methods of etching nitride MAX phases lies in higher energies needed to extract "A" atoms from corresponding MAX phase-for example, Al from  $Ti_{n+1}AlN_n$  (34). The nitride MXene sheets can dissolve in HF solution because of their lower stability (35). To date, only a few nitride MXenes have been synthesized, and experimental realization of chloride-terminated nitride MXenes has not been achieved. Our

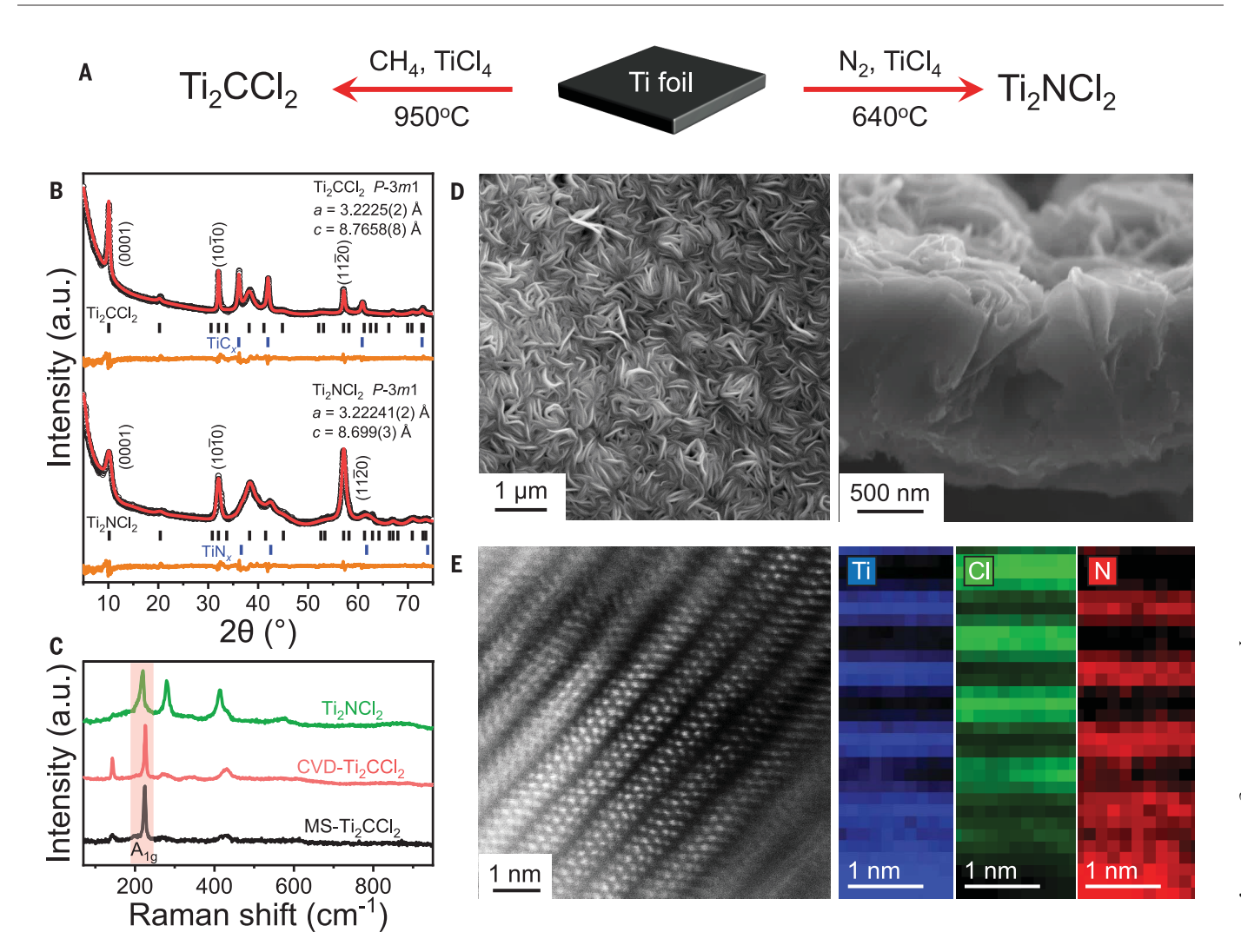


**Fig. 2. CVD growth of MXenes. (A)** Schematic diagram of the CVD reactions. **(B)** XRD patterns and Rietveld refinement for CVD-Ti<sub>2</sub>CCl<sub>2</sub> and CVD-Ti<sub>2</sub>NCl<sub>2</sub>. **(C)** Raman spectra of CVD-Ti<sub>2</sub>CCl<sub>2</sub> and CVD-Ti<sub>2</sub>NCl<sub>2</sub> MXenes in comparison with that of a

traditional MS-Ti<sub>2</sub>CCl<sub>2</sub> MXene, which was synthesized by etching Ti<sub>2</sub>AlC MAX phase with CdCl<sub>2</sub> molten salt. (**D**) Frontal and cross-sectional SEM images of CVD-Ti<sub>2</sub>CCl<sub>2</sub>. (**E**) High-resolution HAADF images and EELS elemental mapping of CVD-Ti<sub>2</sub>NCl<sub>2</sub>.

CVD method, using  $N_2$  as the nitrogen source, further demonstrates the versatility of bottomup MXene syntheses. These reactions can be useful beyond MXenes synthesis. Given that  $TiCl_4$  plays the key role in Ti metallurgy (Kroll process) and in synthesis of  $TiO_2$  from titanium ores (chloride process), both being on the millions of tons annually, the above reactions may create interesting opportunities, such as nitrogen fixation as a side process in conventional  $TiO_2$  synthesis.

# CVD growth of hierarchically structured MXenes

During the CVD synthesis of Ti<sub>2</sub>CCl<sub>2</sub> MXene, gaseous reagents react with the titanium surface (36). As the thickness of growing MXene carpet increases, the diffusion of gaseous reagents toward the reaction zone (Fig. 3A) would slow down, and the growth of the MXene carpet would be expected to be self-limiting.

However, we observed a new growth regime that allowed MXenes to bypass this kinetic bottleneck through the sequence of growth stages captured by ex situ SEM studies (fig. S21) and shown schematically in Fig. 3B. The uniform growth of the MXene carpet (Fig. 2D) was followed by the formation of "bulges" (Fig. 3C) that further evolved into spherical MXene "vesicles" (Fig. 3D). Next, these vesicles detached from the substrate (Fig. 3, F and G). The process could repeat itself, the exposed fresh surfaces enabling continuous synthesis of MXenes. After a prolonged CVD reaction. metal titanium was completely consumed (fig. S22). The internal structure of CVD-MXene vesicles was composed of Ti<sub>2</sub>CCl<sub>2</sub> sheets radiating from the center and oriented normal to the surface (Fig. 3H and fig. S23). Imaging of a fragmented vesicle (Fig. 3E) and individual vesicles dissected with a focused ion beam (FIB) revealed a small void at the vesicle centers (fig. S24). Small  $\mathrm{TiC}_x$  crystallites have been often found around the central void of MXene vesicles (figs. S25 and S26), suggesting that buckling of MXene carpet can be initiated by  $\mathrm{TiC}_x$  nucleated under the growing MXene carpet.

The complexity of hierarchical organization of CVD- ${\rm Ti}_2{\rm CCl}_2$  vesicles is unusual for MXenes. The formation of "flower-like" morphologies—observed, for example, for graphene (37)—typically resulted from anisotropic growth initiated by a spherical seed acting as center. However, in the case of CVD-grown MXenes, spherical vesicles emerged from the planar MXene carpet. Their possible growth mechanism can be derived from a recent theoretical work, inspired by the nonequilibrium evolution of cell and organelle membranes, that illustrated how membrane growth could lead

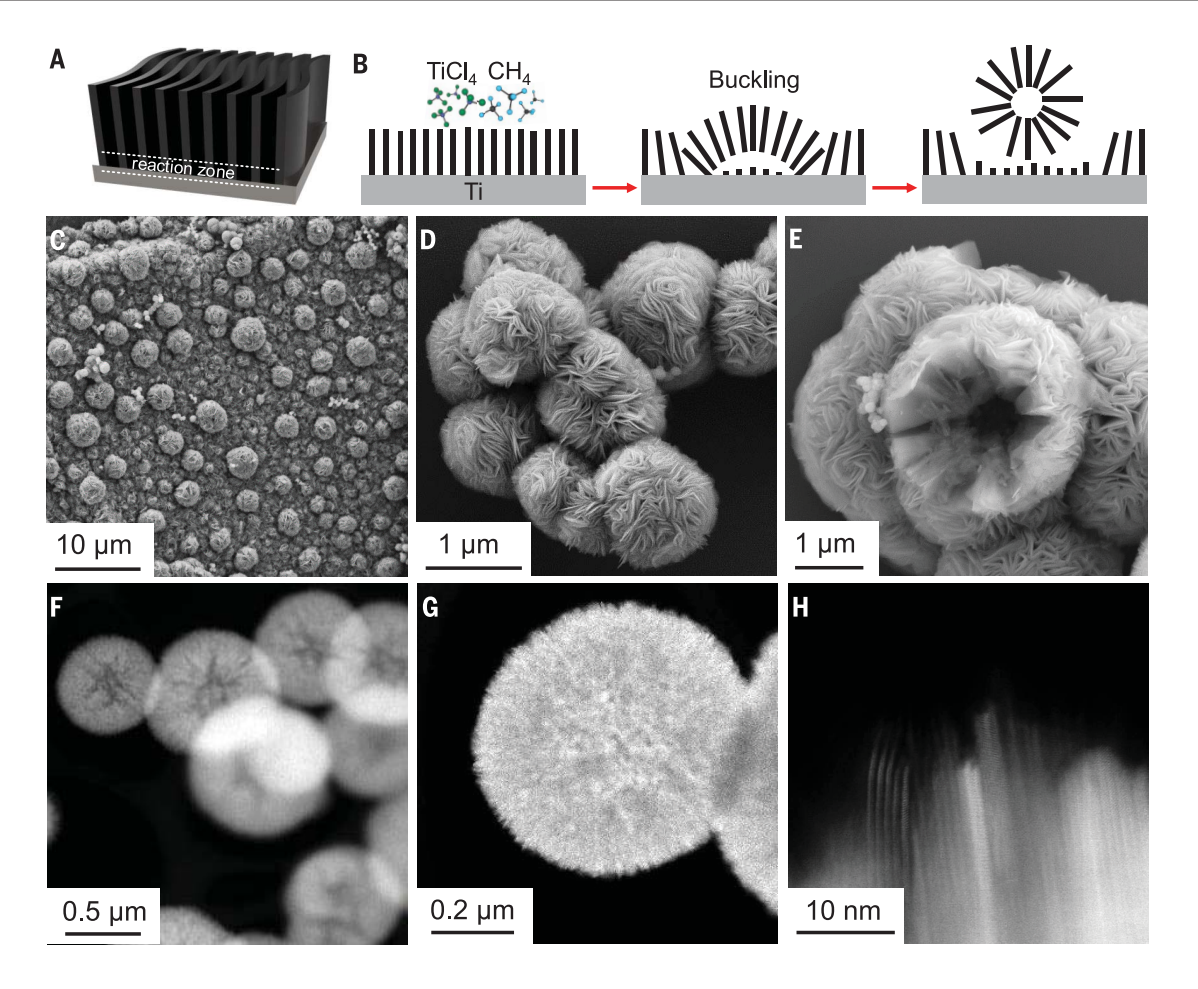


**Fig. 3. Morphologies of CVD-Ti<sub>2</sub>CCl<sub>2</sub>. (A** and **B**) Schematic diagrams illustrating the (A) reaction zone and (B) proposed buckling mechanism of CVD-Ti<sub>2</sub>CCl<sub>2</sub> through which microspheres are formed. (**C** to **E**) SEM images show that morphology of CVD-Ti<sub>2</sub>CCl<sub>2</sub> can be varied by tuning reaction

conditions. (C) Microspheres growing on carpets. (D) Individual microspheres (E) A fragmented microsphere showing a hollow center. ( $\mathbf{F}$  to  $\mathbf{H}$ ) STEM analysis further shows that vertically aligned MXene sheets constitute the microspheres, while a void is left at the center.

to a variety of nontrivial geometries similar to our experimentally observed MXene vesicles (38).

The MXene carpet formed at an early stage of CVD growth (Fig. 2C) and loosely attached to the substrate can be approximated as an elastic 2D membrane. The energetics of such an elastic membrane can be defined through the surface area and local curvature by using a Helfrich Hamiltonian with a surface tension and bending rigidity terms, proportional to the surface tension  $\gamma$  and the bending rigidity  $\kappa$ , respectively (39). When  $\gamma$ ,  $\kappa > 0$ , the membrane naturally prefers a flat geometry under equilibrium conditions (40). However, when new material is constantly added to the sheet, the standard equilibrium description fails to predict its shape and stability (41). During a CVD process, new MXene sheets keep nucleating and growing on the surface of Ti foil. The addition of new materials to a substrate with a fixed area creates substantial in-plane stress within MXene carpet, which can be relaxed by out-of-plane wrinkling or buckling where flexible MXene carpet detaches from rigid Ti surface (42, 43). Viewed in the context of the above-described elastic sheet model, the growth of MXenes induced a negative surface tension in an effective free-energy landscape (supplementary text 2).

Van der Waals-bonded 2D MXene sheets can efficiently slide against each other, which creates only a small elastic penalty for the formation of buckled and curved geometries. Ultimately, these deformations can collapse into spherical vesicles that detach and refresh the substrate for further growth, as schematically shown in Fig. 3B. We found that gas reagent flow rate has a strong effect on the morphology of the CVD product. Flat carpets and bulges were favored at different flow rates (fig. S27), further suggesting that hierarchical morphology of CVD-grown MXenes results from the interplay of complex reaction kinetics rather than from templated growth. We emphasize that detailed mechanistic understanding of MXene vesicles growth will require additional computational and experimental studies. We simply propose a plausible mechanism to help explain the observed phenomenology.

# **Electrochemical energy storage**

MXenes are known for their excellent pseudocapacitive energy storage properties that stem from the combination of large surface-tovolume ratio and high electrical conductivity. Ti<sub>2</sub>CT<sub>x</sub> MXenes show some of the highest predicted and experimentally observed capacities among all studied MXene materials (20, 44). We investigated the Li-ion storage properties of electrodes prepared from DS-Ti<sub>2</sub>CCl<sub>2</sub> and CVD-Ti<sub>2</sub>CCl<sub>2</sub>. We performed electrochemical characterizations on DS-Ti<sub>2</sub>CCl<sub>2</sub> using a two-electrode (Li coin cell) configuration. A conducting additive, 10 wt % Super P carbon black, was added following the standard approach. The first several cyclic voltammetry (CV) cycles of a delaminated DS-Ti<sub>2</sub>CCl<sub>2</sub> electrode recorded at a scan rate of 0.5 mV·s<sup>-1</sup> within the electrochemical potentials from 0.2 to 3.0 V versus Li+/Li (fig. S28A) showed

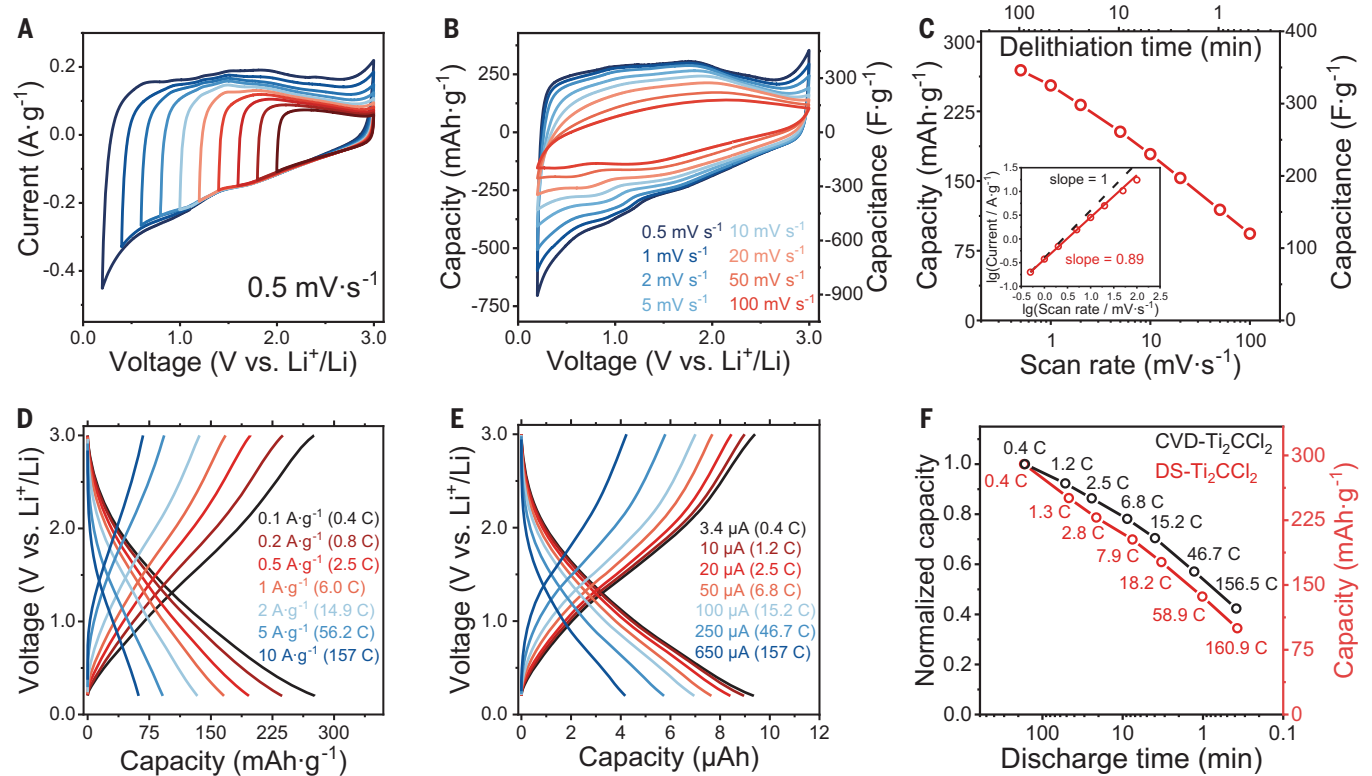


**Fig. 4. Electrochemical energy storage properties of Ti<sub>2</sub>CCl<sub>2</sub> MXenes.**(**A**) Cyclic voltammetry (CV) profiles of delaminated DS-Ti<sub>2</sub>CCl<sub>2</sub> with various negative cut-off potentials at a scan rate of  $0.5 \text{ mV} \cdot \text{s}^{-1}$ . (**B**) CV profiles of delaminated DS-Ti<sub>2</sub>CCl<sub>2</sub> at different scan rates from  $0.5 \text{ to } 100 \text{ mV} \cdot \text{s}^{-1}$ . Differential capacity *Q* was derived from differential capacitance *C*. (**C**) Change of DS-MXene electrode capacity and capacitance versus the discharge time during CV scan recorded at

various potential scan rates. (Inset) *b*-value determination. (**D**) Galvanostatic charge-discharge (GCD) profiles of DS-Ti<sub>2</sub>CCl<sub>2</sub> from current densities of 0.1 to 10 A·g<sup>-1</sup>. (**E**) GCD profiles of CVD-Ti<sub>2</sub>CCl<sub>2</sub> from current densities of 3.4 to 650  $\mu$ A. (**F**) Normalized galvanostatic discharge capacity of CVD-Ti<sub>2</sub>CCl<sub>2</sub> and DS-Ti<sub>2</sub>CCl<sub>2</sub> electrodes from 0.4 to ~160 C. Absolute capacity of DS-Ti<sub>2</sub>CCl<sub>2</sub> is shown in the secondary *y* axis as a reference.

redox peaks that can be assigned to the formation of a solid electrolyte interphase (SEI) layer (4, 45). After the third CV cycle, the specific capacitance of DS-MXene electrode stabilized at 341  $\rm F\cdot g^{-1}$  (which corresponds to a capacity of 265 mA-hour- $\rm g^{-1}$ ) (fig. S28B), which is in a good agreement with previously reported data for MS-Ti<sub>2</sub>CCl<sub>x</sub> MXene (44). The rectangular CV profile without redox peaks suggests a pseudocapacitive energy storage mechanism for delaminated MXenes (46), which is further supported by the consistency of the rectangular CV profiles recorded with different negative cut-off potentials (Fig. 4A).

The charge storage kinetics were investigated by measuring the dependence of electrochemical current i on the potential scan rate v (supplementary text 3). In theory, the current scales with scan rate as  $i \sim v^b$ , where a b-value of 1 corresponds to a capacitive process, and a b-value of 0.5 is typical for battery-type energy storage (47). CV profiles of delaminated DS-Ti<sub>2</sub>CCl<sub>2</sub> MXene at scan rates from 0.5 to 100 mV·s<sup>-1</sup> are shown in Fig. 4B. The specific lithiation capacities and capacitances, versus charge-discharge times and scan rates

calculated from the CV profiles, are plotted in Fig. 4C. The Fig. 4C inset shows the iversus v plotted in logarithmic scale from 0.5 to 100 mV·s<sup>-1</sup>. We observed a linear relationship with a slope of  $b \approx 0.89$  for scan rates that ranged from 0.5 to 20 mV·s<sup>-1</sup>, indicating a capacitive-like charge storage for the delaminated DS-Ti<sub>2</sub>CCl<sub>2</sub> electrodes. Galvanostatic charge-discharge (GCD) profiles of a DS-Ti<sub>2</sub>CCl<sub>2</sub> electrode are shown Fig. 4D. About 48% capacity was maintained from a current density of 0.1 to 2 A·g<sup>-1</sup>, which is comparable with previously reported values for Cl-terminated MXenes (44, 48). A maximum capacity of 286 mA·hour·g<sup>-1</sup> was recorded at a specific current of 0.1 A·g<sup>-1</sup> within 0.1 to 3.0 V (fig. S29), which is slightly higher than previously reported value for the optimized performance of MS-Ti<sub>2</sub>CCl<sub>2</sub> MXene (44). These electrochemical studies further confirm excellent electrochemical characteristics of DS-Ti<sub>2</sub>CCl<sub>2</sub> MXene.

The high-rate performance of MXenes is sensitive to electrode microstructure such as flake size, flake orientation, and pore size distribution (49). For example, restacking of ex-

foliated MXene sheets can reduce the surface area that is easily accessible for intercalating ions, which is a well-known problem of 2D materials (50). New morphologies, such as CVD-grown MXene carpets and vesicles with individual sheets oriented normal to the substrate (Fig. 3), can facilitate the development of MXenes for fast electrochemical energy storage. To preserve the as-synthesized morphology, CVD-Ti<sub>2</sub>CCl<sub>2</sub> grown on Ti foil (fig. S30) was directly used as an electrode for an electrochemical cell. Galvanostatic plots at various current densities highlight the high-power performance of CVD-Ti<sub>2</sub>CCl<sub>2</sub> electrode with vertically oriented MXene sheets in Li+ intercalation processes (Fig. 4E). The CVD electrode further shows a slightly better high-rate performance than that of delaminated MXene from 0.4 C to ~160 C (Fig. 4F). The b-value of CVD-Ti<sub>2</sub>CCl<sub>2</sub> was calculated as 0.93 (fig. S31D), which indicates an energy storage mechanism closer to that of a freely diffusing capacitor. A better understanding of ion transport in complex morphologies of CVD-grown MXenes, as well as charge transport between individual MXene vesicles, should help to further optimize the electrochemical performance of DS- and CVD-grown MXenes.

#### **REFERENCES AND NOTES**

- 1. M. Naguib et al., Adv. Mater. 23, 4248-4253 (2011).
- J. Halim et al., Chem. Mater. 26, 2374-2381 (2014).
- M. Ghidiu, M. R. Lukatskaya, M. Q. Zhao, Y. Gogotsi, M. W. Barsoum, Nature 516, 78-81 (2014).
- Y. Li et al., Nat. Mater. 19, 894-899 (2020)
- V. Kamysbayev et al., Science 369, 979-983 (2020).
- 6. O. Mashtalir et al., Nat. Commun. 4, 1716 (2013).
- Y. Xia et al., Nature 557, 409-412 (2018).
- M. Naguib et al., J. Am. Chem. Soc. 135, 15966-15969 8.
- A. Igbal et al., Science 369, 446-450 (2020)
- 10. F. Shahzad et al., Science 353, 1137-1140 (2016).
- 11. K. Hantanasirisakul et al., Adv. Electron. Mater. 2, 1600050 (2016).
- 12. H. Zhou et al., Nat. Commun. 12, 5510 (2021).
- 13. M. A. Hope et al., Phys. Chem. Chem. Phys. 18, 5099-5102
- G. R. Bhimanapati et al., ACS Nano 9, 11509-11539 (2015).
- 15. M. Naguib et al., ACS Nano 6, 1322-1331 (2012).
- J. Zhou et al., Angew. Chem. Int. Ed. 55, 5008-5013
- J. Halim et al., Adv. Funct. Mater. 26, 3118-3127
- 18. D. L. Druffel et al., Chem. Mater. 31, 9788-9796 (2019).
- S. J. Hwu, R. P. Ziebarth, S. Vonwinbush, J. E. Ford, J. D. Corbett, Inorg. Chem. 25, 283-287 (1986).
- 20. B. Anasori, M. R. Lukatskaya, Y. Gogotsi, Nat. Rev. Mater. 2, 16098 (2017).
- 21. A. VahidMohammadi, J. Rosen, Y. Gogotsi, Science 372, 1165-1178 (2021).
- 22. X. L. Li et al., Adv. Energy Mater. **10**, 2001394 (2020). 23. H. Wang et al., Adv. Mater. **30**, e1704561 (2018).
- 24. C. J. Zhang et al., Chem. Mater. 29, 4848-4856 (2017).
- 25. Y. R. Luo et al., Joule 3, 279-289 (2019).
- 26. X. Yang, N. Gao, S. Zhou, J. Zhao, Phys. Chem. Chem. Phys. 20, 19390-19397 (2018).
- 27. V. Natu et al., Matter 4, 1224-1251 (2021)
- 28. D. Voiry et al., Nat. Chem. 7, 45-49 (2015).

- 29. C. Xu et al., Nat. Mater. 14, 1135-1141 (2015).
- 30. Y. L. Hong et al., Science 369, 670-674 (2020).
- 31. O. Ledain et al., Phys. Procedia 46, 79-87 (2013).
- 32. C. Stern et al., Sci. Rep. 8, 16480 (2018).
- 33. H. Kumar et al., ACS Nano 11, 7648-7655 (2017).
- 34. I. R. Shein, A. L. Ivanovskii, Comput. Mater. Sci. 65, 104-114
- 35. M. Naguib, V. N. Mochalin, M. W. Barsoum, Y. Gogotsi, Adv. Mater. 26, 992-1005 (2014).
- 36. J. Gavillet et al., Phys. Rev. Lett. 87, 275504 (2001).
- 37. S. Y. Wang et al., Carbon 120, 103-110 (2017).
- 38. J. Binysh, T. R. Wilks, A. Souslov, Sci. Adv. 8, eabk3079 (2022).
- 39. G. Salbreux, F. Jülicher, Phys. Rev. E 96, 032404 (2017).
- 40. A. D. Pezzutti, H. Hernández, J. Phys. Conf. Ser. 1603, 012003 (2020)
- 41. Z. Hua et al., Nat. Commun. 10, 5406 (2019).
- 42. B. Li, Y. P. Cao, X. Q. Feng, H. J. Gao, Soft Matter 8, 5728-5745 (2012).
- 43. D. J. Schmidt et al., ACS Nano 3, 2207-2216 (2009).
- 44. G. Ma et al., Nat. Commun. 12, 5085 (2021).
- 45. R. M. Gnanamuthu, C. W. Lee, Mater. Chem. Phys. 130, 831-834 (2011).
- 46. S. Fleischmann et al., Nat. Energy 7, 222-228 (2022).
- 47. N. Elgrishi et al., J. Chem. Educ. 95, 197-206 (2018).
- 48. L. Liu et al., ACS Nano 16, 111-118 (2022).
- 49. M. R. Lukatskaya et al., Nat. Energy 2, 17105 (2017).
- 50. J. Wang, V. Malgras, Y. Sugahara, Y. Yamauchi, Nat. Commun. 12, 3563 (2021).

#### **ACKNOWLEDGMENTS**

The authors express their appreciation to I. Golovina for helping with atomic force microscopy measurements. We thank Y. Han and G. Yan for helpful discussions about electrochemical measurements and G. Olack for helping with SEM data analysis. We are also grateful to A. Nelson for a critical reading and editing of the manuscript and M. Talapin for help with artwork. Funding: The work on direct MXene synthesis was supported by the National Science Foundation under award DMR-2004880, and CVD synthesis was supported by the US Department of Defense Air Force Office of Scientific Research under grants FA9550-22-1-0283 and FA9550-20-1-0104. Electrochemical studies were supported by the Advanced Materials for Energy-Water Systems (AMEWS) Center, an Energy Frontier Research Center funded by the US Department of Energy (DOE), Office of Science, Basic Energy Sciences. W.C. and S.V. were supported by the University of Chicago Materials Research Science and Engineering Center, which is funded by the National Science Foundation under award DMR-2011854 S.V. acknowledges support from the National Science Foundation under grant DMR-1848306. F.L. and R.F.K. at UIC were supported by a grant from the National Science Foundation (NSF-DMR 1831406). Acquisition of UIC JEOL ARM200CF was supported by an MRI-R2 grant from the National Science Foundation (DMR-0959470). The Gatan Continuum GIF acquisition at UIC was supported by an MRI grant from the National Science Foundation (DMR-1626065). FIB-SEM was performed at the Canadian Centre for Electron Microscopy, a Canada Foundation for Innovation Major Science Initiatives funded facility. The work also used resources of the Center for Nanoscale Materials, a DOE Office of Science User Facility operated for the DOE Office of Science by Argonne National Laboratory under contract DE-AC02-06CH11357. Author contributions: D.W. performed and designed the experiments analyzed data, and cowrote the paper. C.Z. carried out Raman measurements and data analysis. A.S.F. contributed to x-ray measurements and data analysis. W.C. contributed to TEM analysis of delaminated MXene and building the CVD system. F.L. and R.F.K. performed high-resolution STEM studies and image analysis. M.W. and C.L. contributed to the electrochemistry measurements and data analysis. S.V. performed simulations and interpretation of the morphology of CVD-MXenes. D.V.T. conceived and designed experiments and simulations, analyzed data, cowrote the paper. and supervised the project. All authors discussed the results and commented on the manuscript. Competing interests: D.W. and D.V.T. are inventors on patent application US 63/399,931 submitted by the University of Chicago, which covers direct synthesis and CVD of MXenes. Data and materials availability: All data needed to evaluate the conclusions in the paper are present in the paper or the supplementary materials. The samples can be provided by the authors upon reasonable request under a materials transfer agreement with the university. Correspondence and requests for materials should be addressed to D.V.T. (dytalapin@uchicago.edu), License information: Copyright © 2023 the authors, some rights reserved; exclusive licensee American Association for the Advancement of Science. No claim to original US government works. https://www.science.org/about/ science-licenses-journal-article-reuse

# SUPPLEMENTARY MATERIALS

science.org/doi/10.1126/science.add9204 Materials and Methods Supplementary Notes Figs. S1 to S34 Tables S1 to S5 References (51-59)

Submitted 13 July 2022; accepted 31 January 2023 10.1126/science.add9204



# Direct synthesis and chemical vapor deposition of 2D carbide and nitride MXenes

Di Wang, Chenkun Zhou, Alexander S. Filatov, Wooje Cho, Francisco Lagunas, Mingzhan Wang, Suriyanarayanan Vaikuntanathan, Chong Liu, Robert F. Klie, and Dmitri V. Talapin

Science, 379 (6638), .

DOI: 10.1126/science.add9204

# **MXenes without MAX phases**

Two-dimensional metal carbides and nitrides, or MXenes, have several potential applications in energy storage and electronics. They are usually made by delamination of a layered parent compound, a MAX phase, in a harsh etching step. Wang *et al.* synthesized one of the most widely used MXenes, Ti<sub>2</sub>CCl<sub>2</sub>, as well as MXenes not available from MAX phases, using chemical vapor deposition (see the Perspective by Robertson and Tolbert). The reaction of methane and titanium tetrachloride on a titanium surface led to the growth of Ti<sub>2</sub>CCl<sub>2</sub> sheets perpendicular to the metal. Under some growth conditions, the sheets could buckle off the surface to form vesicles. —PDS

# View the article online

https://www.science.org/doi/10.1126/science.add9204

**Permissions** 

https://www.science.org/help/reprints-and-permissions

Use of this article is subject to the Terms of service